Arabian Journal of Chemistry (2022) **15**, 103842

King Saud University

Arabian Journal of Chemistry

www.ksu.edu.sa
www.sciencedirect.com

ORIGINAL ARTICLE

Cytotoxicity, antifungal, antioxidant, antibacterial and photodegradation potential of silver nanoparticles mediated via *Medicago sativa* extract

Majid Zare-Bidaki [a], Hamed Aramjoo [b], Zirar M. Mizwari [c,d], Pouria Mohammadparast-Tabas [b], Reyhane Javanshir [b], Sobhan Mortazavi-Derazkola [e,*]

[a] *Infectious Diseases Research Center, Birjand University of Medical Sciences, Birjand, Iran*
[b] *Student Research Committee, Birjand University of Medical Sciences, Birjand, Iran*
[c] *Department of Medical Laboratory Technology, Shaqlawa Technical College, Erbil Polytechnic University, Erbil, Iraq*
[d] *Rwandz Private Technical Institute, Erbil, Iraq*
[e] *Medical Toxicology and Drug Abuse Research Center (MTDRC), Birjand University of Medical Sciences, Birjand, Iran*

Received 28 January 2022; accepted 13 March 2022
Available online 16 March 2022

KEYWORDS

Silver nanoparticle;
Green synthesis;
Antibacterial;
Cytotoxicity;
Photocatalytic degradation

Abstract The biosynthesis of metallic nanoparticles is on a sharp rise as they have growing applications in environmental and biomedical sciences. This study reports an eco-friendly and cost-effective methodology for synthesizing biogenic silver nanoparticles (AgNPs) using the extract of *Medicago sativa* (*M. sativa*) cultivated in South Khorasan. The parameters used in the synthesis process were optimized to obtain uniformly distributed AgNPs in suitable sizes. The morphological, structural, and bonding characteristics of *M. sativa* extract-based AgNPs (*MSE*-AgNPs) were explored using FTIR, FESEM, EDS, TEM, XRD, UV–Vis, and DLS techniques. UV–Vis spectroscopy confirmed the formation of *MSE*-AgNPs by observing the typical surface plasmon resonance (SPR) peak at 419 nm. XRD, FESEM, TEM, and DLS analyses confirmed the formation of face-centered cubic (fcc) crystalline structure, spherical/elliptical morphology, the average particle size of 15–35 nm, and highly stable *MSE*-AgNPs. Green synthesized *MSE*-AgNPs indicated a significant antioxidant activity (78%) compared to *M. sativa* extract (32%). As such, the synthesized *MSE*-AgNPs revealed a potential antioxidant activity towards the DPPH radicals. The biologically synthesized *MSE*-AgNPs exhibited highly potential antibacterial and antifungal activities against *Pseudomonas aeruginosa*, *Klebsiella pneumoniae*, *Escherichia coli*, *Staphylococcus epidermidis*, *Ente-*

* Corresponding author.
E-mail addresses: S.mortazavi23@yahoo.com, Sobhan.mortazavi@bums.ac.ir (S. Mortazavi-Derazkola).
Peer review under responsibility of King Saud University.

Production and hosting by Elsevier

https://doi.org/10.1016/j.arabjc.2022.103842

rococcus faecalis, *Staphylococcus aureus*, and *Candida albicans* with the minimum inhibitory concentration (MIC) values of 62.5, 125, 125, 1000, 125, 1000, and 31.25 μg/mL, respectively. In vitro cytotoxicity of the *MSE*-AgNPs against human fibroblast (HF) cells indicated a dose–response activity (with IC50 value of 18 μg/mL). Moreover, the AgNPs revealed efficient photocatalytic degradation of thymol blue (TB) as an anionic dye and malachite green (MG) as a cationic dye under sunlight and UV irradiations. Up to 94.37% and 90.12% degradation rates were obtained for MG and TB within only 100 min of UV irradiation. These observations signify that synthesized *MSE*-AgNPs can have great potential for biological and environmental applications.

1. Introduction

Nanotechnology is advancing rapidly due to its wide biological applications, for instance, solar energy capture and conversion, pharmacy, medicine, waste management, catalysts, and sensor design technology (Ghoreishi et al., 2017; Shirzadi-Ahodashti et al., 2020; Zamarchi and Vieira, 2021; Ahmadi et al., 2020; Mohammadzadeh et al., 2019). Additionally; nanoparticles are used effectively for targeted drug delivery, wound healing, production of antimicrobial compound, and the diagnosis and treatment of various diseases such as heart disease (Liu et al., 2017). Today; nanoparticles are utilized in over 1,200 commercial products, including drugs, food preservatives, textiles, and various electronic devices (Abbott Chalew et al., 2013). In 2017; Watermann *et al*. used mesoporous silica nanoparticles as carriers of anti-cancer drugs (Watermann and Brieger, 2017). In 2018; Chen *et al*. produced color sensors based on gold nanoparticles to detect food contaminants rapidly (Chen et al., 2018).

Drawing on chemical and electrochemical materials, researchers have explored several approaches to preparing nanoparticles during the past decade. However, the majority of the current chemical techniques are problematic because they generate hazardous byproducts or require a great deal of energy (Kim et al., 2007). To address the pollution associated with these methods, researchers have proposed ecologically friendly approaches using biological principles that incorporate microorganisms or plant extracts in the synthesis process (Ravichandran et al., 2019). There is evidence that plant extracts reduce metal ions more rapidly and with greater stability than microbes (Bagherzade et al., 2017). Nanoparticles are manufactured using a variety of metals, including gold (Ebrahimzadeh et al., 2020; Khoshnamvand et al., 2020), silver (Shirzadi-Ahodashti et al., 2021; Huo et al., 2019), iron (Zhou et al., 2021), and zinc (V. k, v. a, m. p, s. s, m. s, s. s, 2022). In 2020, Awwad et al. biosynthesized zinc oxide nanoparticles 5 to 15 nm in spherical shape using Ailanthus altissima fruit (Awwad et al., 2020). In 2017, Bagherzade et al. used Crocus sativus extract to produce silver nanoparticles (AgNPs) with an average size of 15 nm and a spherical shape (Bagherzade et al., 2017).

Silver is one of the most widely used metals with multiple properties (Mittal et al., 2014). The simple biosynthesis, low cost, fast production, and effective anticancer and antibacterial properties of AgNPs have made silver one of the foremost materials employed in nanoparticle biosynthesis (AlSalhi et al., 2019). AgNPs are synthesized using biological sources, especially plant materials, and are small in size and large in surface (Ahmed et al., 2016). Numerous plant-based biological techniques for the intracellular and extracellular synthesis of AgNPs have been documented (Shirzadi-Ahodashti et al., 2020; Ebrahimzadeh et al., 2021; Hidayat et al., 2022). Spherical AgNPs with a diameter of 50–60 nm have been synthesized using *Thymus kotschyanus* plant extract and demonstrated to have remarkable antioxidant and antibacterial effects against *Escherichia coli*; *Pseudomonas aeruginosa*; *Staphylococcus aureus,* and *Bacillus subtilis* (Hamelian et al., 2018). AgNPs synthesized with sesame oil cake exhibit significant anticancer properties against breast cancer cell lines (MCF-7) (Alfuraydi et al., 2019). Moreover, green AgNPs derived from *Moringa oleifera* seed extract display significant photocatalytic properties against organic dyes such as methylene blue, and 4-nitrophenol (Mehwish et al., 2021).

Alfalfa (*Medicago sativa*), also known as lucerne or purple medic, is the most widely cultivated forage plant in Iran many other countries of the globe and is referred to as the "queen of forage plants" owing to its high nutritional value and ease of production. *Medicago sativa* is one of the largest genera of legumes (Fabaceae) distributed in Iran. The genus, which is thought to have originated in southern or northern Iran, has 34 annual and 51 perennial species and constitutes Iran's principal forage crop (Basafa and Taherian, 2009). Medicago sativa is widely used as a perennial forage plant due to its high protein content and bulk biomass. Approximately 32.2 million hectares of Medicago sativa are annually planted worldwide (Shi et al., 2017). The plant can be a suitable candidate for biological and environmental applications because of its great potential.

The significance and efficacy of nanoparticles are determined by their morphology, size, and stability, all of which are directly related to the compound's synthesis method. Nanoparticles with a high surface-to-volume ratio display novel and unique properties. This study aimed to develop a suitable method for the *Medicago sativa*-based biosynthesis of AgNPs and investigate their cytotoxic, catalytic, antibacterial, antifungal, and antioxidant properties.

2. Material and method

2.1. Materials and equipment

Silver nitrate ($AgNO_3$; USA) and methanol (CH_3OH; Germany) were purchased from Sigma and Merck companies, respectively. In all experiments, deionized distilled water was used as a solvent for silver nitrate and plant extract. Standard strains of three species of Gram-positive bacteria, including *Staphylococcus aureus* (ATCC 29213; *S. aureus*), *Staphylococcus epidermidis* (ATCC 12228; *S. epidermidis*), and *Enterococcus faecalis* (ATCC 29212; *E. faecalis*) and three species of Gram-negative bacteria, including *Escherichia coli* (ATCC 25922; *E. coli*), *Pseudomonas aeruginosa* (ATCC27853; *P. aeruginosa*), and *Klebsiella pneumoniae* (ATCC 9997; *K. pneumoniae*) as well as one standard strain of *Candida albicans* (ATCC 10231; *C. albicans*) were used for antibacterial and antifungal studies. All were purchased from the Pasteur Institute of Iran. Moreover, ceftriaxone and amphotericin B were employed to compare the antibacterial and antifungal effects, respectively.

2.2. Preparation of Medicago sativa extract

Medicago sativa was collected and approved by the Herbarium Department of Birjand University, washed with distilled water,

dried in the shade, and ground to yield powder. Subsequently, 25 g of the plant powder was stirred with 500 mL of methanol for 72 h at room temperature. The resultant suspension was filtered using a Buchner funnel and a Whatman filter paper, grade 41, before it was placed in a rotary vacuum evaporator. The obtained dried powder was refrigerated at 4 °C until used.

2.3. Green synthesis of silver nanoparticles

Biogenic AgNPs were synthesized according to a previous report (Hashemi et al., 2021). Hence, 16 mg of silver nitrate ($AgNO_3$) was dissolved in 10 mL of deionized distilled water under vigorous stirring at ambient temperature. Afterward, 10 mL of the *M. sativa* extract solution with a 10 mg/ml concentration and pH = 12 (using sodium hydroxide) was added drop-wise to the silver nitrate solution. At this stage, Ag^+ ions were reduced to Ag^0 nanoparticles. This conversion was accompanied by a change in the solution's color from yellow to dark brown. The solution was stirred for 60 min. Moreover, the adsorption of the resultant solution was measured at 300 to 500 nm using UV–Vis for further study. Next, the silver solution was centrifuged at 6000 rpm for 5 min. Finally the product was washed with water to remove extracts and excess ions (three times) and dried. In sum, the bio-reduction of Ag (NO_3) into AgNPs using *M. sativa* extract is as follows:

$$Ag(NO_3) \rightarrow Ag + +NO_3$$

$$Ag + +M.sativa\text{extract} \rightarrow Ag0 \quad (2)$$

2.4. Measurements

Optimal conditions of silver nanoparticles using plant extracts:

To ensure optimal conditions for AgNPs synthesis, we evaluated the three parameters of silver nitrate concentration, reaction time, and reaction temperature using UV–Vis analysis (Table.1). Optimization of silver nitrate concentration: For optimal concentration, different concentrations of silver nitrate, including 3, 5, 10, and 15 mM, were used to synthesize AgNPs. The silver nitrate concentration with the highest absorption at a wavelength of 300 to 500 nm was selected as the optimal concentration for synthesis. Optimization of reaction time: The study built on the optimal concentration of silver nitrate to optimize the reaction time and performed the reaction at 5, 10, 30, 60, and 90 min. Moreover, the adsorption of the solution was investigated. Reaction temperature optimization: After optimal concentration and reaction time were calculated, the synthesis reaction of AgNPs was performed using extracts at different temperatures (room temperature, 65 °C, and 85 °C). Afterward, the optimal time for the formation of AgNPs was obtained by analyzing the obtained absorption diagrams.

2.5. Evaluation of antibacterial and antifungal activities

This study investigated the antibacterial effects of three species of Gram-negative bacteria, including *Escherichia coli (E. coli)*, *Pseudomonas aeruginosa (P. aeruginosa)*, and *Klebsiella pneumoniae (K. pneumoniae)*, and three species of gram-positive bacteria, namely, *Staphylococcus aureus (S. aureus)*, *Staphylococcus epidermidis (S. epidermidis)*, and *Enterococcus faecalis (E. faecalis)*. *Candida albicans* (*C. albicans*) were also used to evaluate the antifungal activity. Ceftriaxone and amphotericin B were used as broad-spectrum antibiotics and antifungal agents, respectively, to evaluate their efficacy to that of synthesized *MSE*-AgNPs. The microdilution broth technique was used to explore the effects of nanoparticles on bacteria and fungi. For this purpose, 100 µL of different concentrations of *MSE*-AgNPs, *M. sativa* extract, ceftriaxone, and amphotericin B were poured into sterile microplate wells. Afterward, 100 µL of Mueller Hinton broth culture medium (MHB, Merck, Germany) containing the desired microbial suspension (equivalent to a dilution of 1:150 to the 0.5 McFarland) was added. Moreover, one well was considered a positive control containing 100 µL of desired microbial suspension in MHB medium (equivalent to a dilution of 1:150 to the 0.5 McFarland) and 100 µL of sterile physiology serum. Another well was regarded as a negative control containing only 200 µL of MHB medium. After 24 h, the turbidity of the wells was examined to evaluate the minimum inhibitory concentration (MIC). To evaluate the minimum bactericidal/fungicidal concentration (MBC, MFC), we cultured 10 µL of wells with MIC and higher concentrations on a blood agar medium (Merck, Germany) and incubated for 24 h. Subsequently, the concentration at which no growth was observed on the blood agar medium was selected as the minimum bactericidal/fungicidal concentration. All steps were reiterated three times to reach more robust results.

2.6. Evaluation of the antioxidant activity of MSE-AgNPs by DPPH assay

In this study, the free radical scavenging capacity was investigated through the 1,1-Diphenyl-2-picrylhydrazyl (DPPH) radical method using a Zantox kit (Kavosh Arian Azma Co., Iran) (Brand-Williams et al., 1995). In this method, 10 µL of *M. sativa* extract samples (in concentrations of 5, 2, and 1 mg/mL), *MSE*-AgNPs (in concentrations of 43, 17.2, and 8.6 µg/mL), control sample (available in the kit), distilled water (blank sample), and various standards (in concentrations of 62.5, 125, 250, 500, and 1000 µM) were poured into micro-wells. Afterward, 250 µL of the prepared 1,1-Diphenyl-2-picrylhydrazyl solution was added to each of the micro-wells, and the plate was shaken for 30 s. Eventually, the plate was incubated for 20 min at room temperature. Typically, When DPPH radicals are dissolved in an organic solvent, they undergo a color change into purple that may be detected using a spectrophotometer at 517 nm. As the concentration of reducing compounds increases, the purple color fades more rapidly. The results of this test were reported as the percentage of DPPH radical inhibition. The following equation was used to compute the radical scavenging capacity of DPPH:

$$DPPHradicalscavenging(\%) = [(A_0 - A_1)/A_0] \times 100 \quad (3)$$

where A_0 is the absorbance of the DPPH solution, and A_1 is the absorbance of the sample.

2.7. Evaluation of cytotoxicity MSE-AgNPs

Human fibroblast cells were obtained from the cell bank of the cell bank in Pasteur Institute of Iran. The cells were grown to 80–90% confluence in a culture plate with the DMEM medium

Table 1 Experimental detail for biosynthesis of silver nanoparticles using *M. sativa* extract.

Sample no.	Ag concentration (mM)	Time (min)	Temperature (°C)	Figure of UV
1	3	60	Room temp.	Fig. 1a
2	5	60	Room temp.	Fig. 1a
3	10	60	Room temp.	Fig. 1a
4	15	60	Room temp.	Fig. 1a
5	10	5	Room temp.	Fig. 1b
6	10	10	Room temp.	Fig. 1b
7	10	30	Room temp.	Fig. 1b
8	10	90	Room temp.	Fig. 1b
9	10	60	65	Fig. 1c
10	10	60	85	Fig. 1c

including streptomycin (100 µg/mL), penicillin (100 U/mL) and fetal bovine serum (FBS; 10%) at 37 °C. Then, the impact of *MSE*-AgNPs at different concentrations (3, 5, 12.5, 25, 50, 100 µg/mL) on fibroblast cell viability was determined for 24 h. MTT (Sigma, USA) staining was used to assess the cytotoxicity of the synthesized AgNPs on human fibroblasts. At first, the cell suspension was prepared from normal cells, and 200 µL of this suspension was added to each well from 96 house plates. Ten thousand cells were implanted in cell culture plates and treated with AgNPs concentrations of 3, 5, 12.5, 25, 50, 100 µg/mL. After 24 h, 20 µL of MTT dye (with a final concentration of 5 mg/ml) was added to the wells and incubated for 5 h at 37° C with 5% CO_2. The supernatant solution was discarded, and the formed formazan crystals were dissolved in 150 µL of DMSO. Additionally, the absorbance of the wells at 570 nm was read using an ELISA reader (Epoch, Biotek USA). The cell viability percentage was calculated as follows:

$$Cellviability(\%) = (sampleabsorption/controlabsorption) \times 100$$

2.8. Investigation of the catalytic performance of MSE-AgNPs

The photocatalytic activity of the synthesized *MSE*-AgNPs occurred in sunlight and under UV irradiation. Different amounts of dyes as contaminants (5 ppm) were diluted in distilled water and poured into a beaker. A certain amount of biosynthesized *MSE*-AgNP*s* (35 mg) was added to the solution containing the dye. Before irradiation, the solution was aerated with oxygen (for equilibrium adsorption and desorption) under dark conditions for 30 min. The solution in the beaker was sampled after some time, and a UV–Vis optical spectrometer was employed to measure its adsorption (at specific times). The percentage of pollutant degradation was determined: Degradation (%) = $(A_0\text{-}A_t)/A_t*100$ (5), where A_0 is the initial adsorption and A_t is the adsorption at time t.

2.9. Characterization

The FT-IR (PerkinElmer Spectrum TwoTM IR spectrometer; Model L160000U) test was adopted to evaluate the functional groups of samples. Moreover, XRD analysis was used at an angle 2θ = 10–80° (Philips PW1800 using CuKα radiation) to determine the synthesized particles' crystal structure and size. The formation of AgNPs with UV–Vis spectrum was confirmed using a Nanodrop device (BioTek model Epoch; USA). Particle size and surface charge of synthesized nanoparticles were confirmed by DLS and zeta potential (NanoBrook 90Plus-Brookhaven Instruments, model 18051; USA). FESEM (TESCAN BRNO-Mira3 LMU) and TEM (Zeiss-EM10C-100 KV) analyses evaluated the synthesized nanoparticles' morphology and size.

2.10. Statistical analysis

At the very least, each experiment was performed in triplicates. Microsoft Excel and the Origin Pro 9 software program were used to determine the whole data. The data were analyzed using a one-way analysis of variance (ANOVA) and the Duncan post-hoc test (P-value < 0.05).

3. Results and discussion

3.1. Optimization of synthesized nanoparticles

In this study, the UV–Vis spectrum at a wavelength of 300–500 nm was employed to validate the formation of AgNPs and analyze the impact of different parameters on the formation of nanoparticles. The intensification of the surface plasmon resonance of silver nanoparticles during the reaction leads to a change in the solution's color to dark brown. This intensification of the surface plasmon creates an absorption band at a wavelength of 300–500 nm. Past results have shown that increasing the absorption rate of nanoparticles is directly related to an increased formation of synthesized nanoparticles (Naghizadeh et al., 2021). Thus, this absorption can be built on to explore the impact of different parameters on the formation of nanoparticles. Effect of silver ion concentration: Silver nitrate concentrations of 3, 5, 10, and 15 mM were examined to identify the optimal concentration for AgNP biosynthesis. Previous research indicates that more nanoparticles are formed with the increase in silver salt (Anand et al., 2017). As shown in Fig. 1a, the intensity of the absorption band increases as the concentration of silver nitrate rises to 10 mM, whereas it decreases after 10 mM. This decline in adsorption intensity can be due to the adhesion of nanoparticles to each other. Hence, the optimal concentration of silver nitrate for further experiments was considered to be 10 mM. Effect of reaction time: Fig. 1b illustrates the UV–Vis absorption spectra of the nanoparticle solution at different times (5, 10, 30, 60, and 90 min). As can be seen, the adsorption intensity increases with

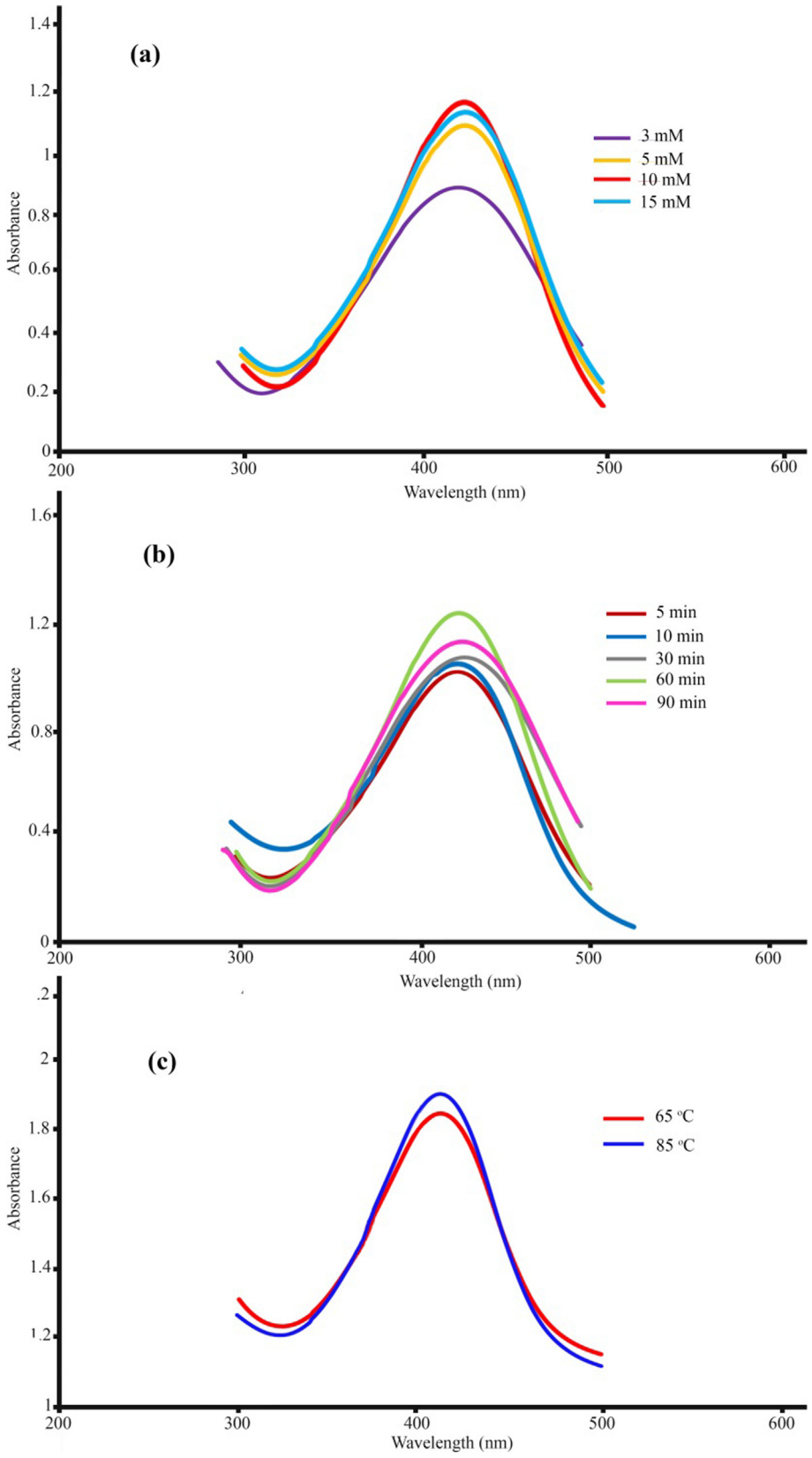

Fig. 1 UV–Vis spectra of as-synthesized silver nanoparticles using *M. sativa* extract: (a) silver nitrate concentration, (b) time, and (c) temperatures.

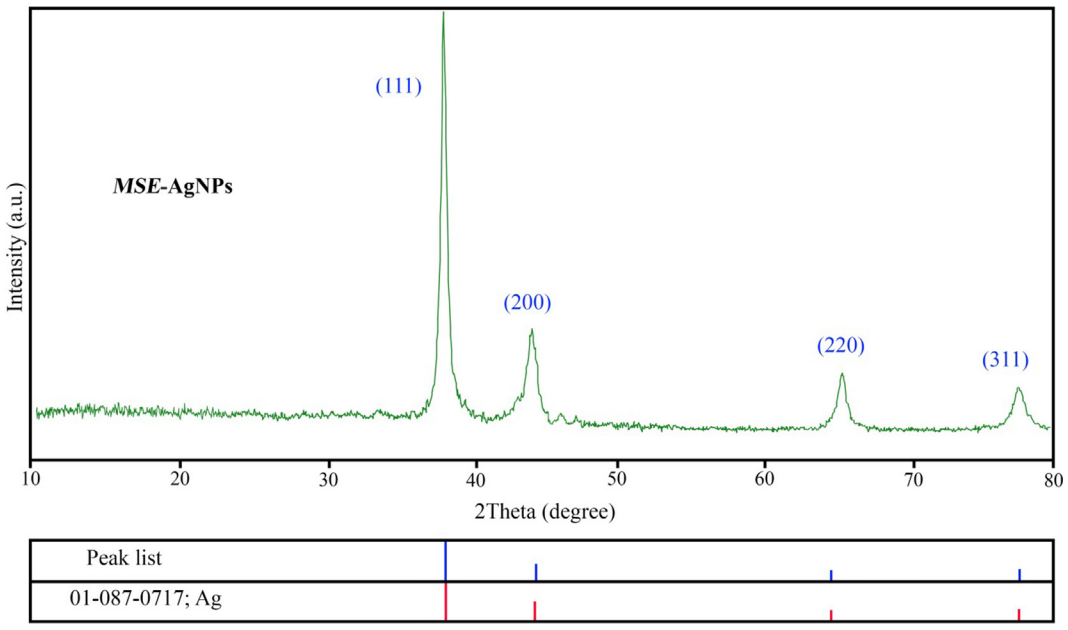

Fig. 2 XRD pattern of *MSE*-AgNPs (sample no. 10).

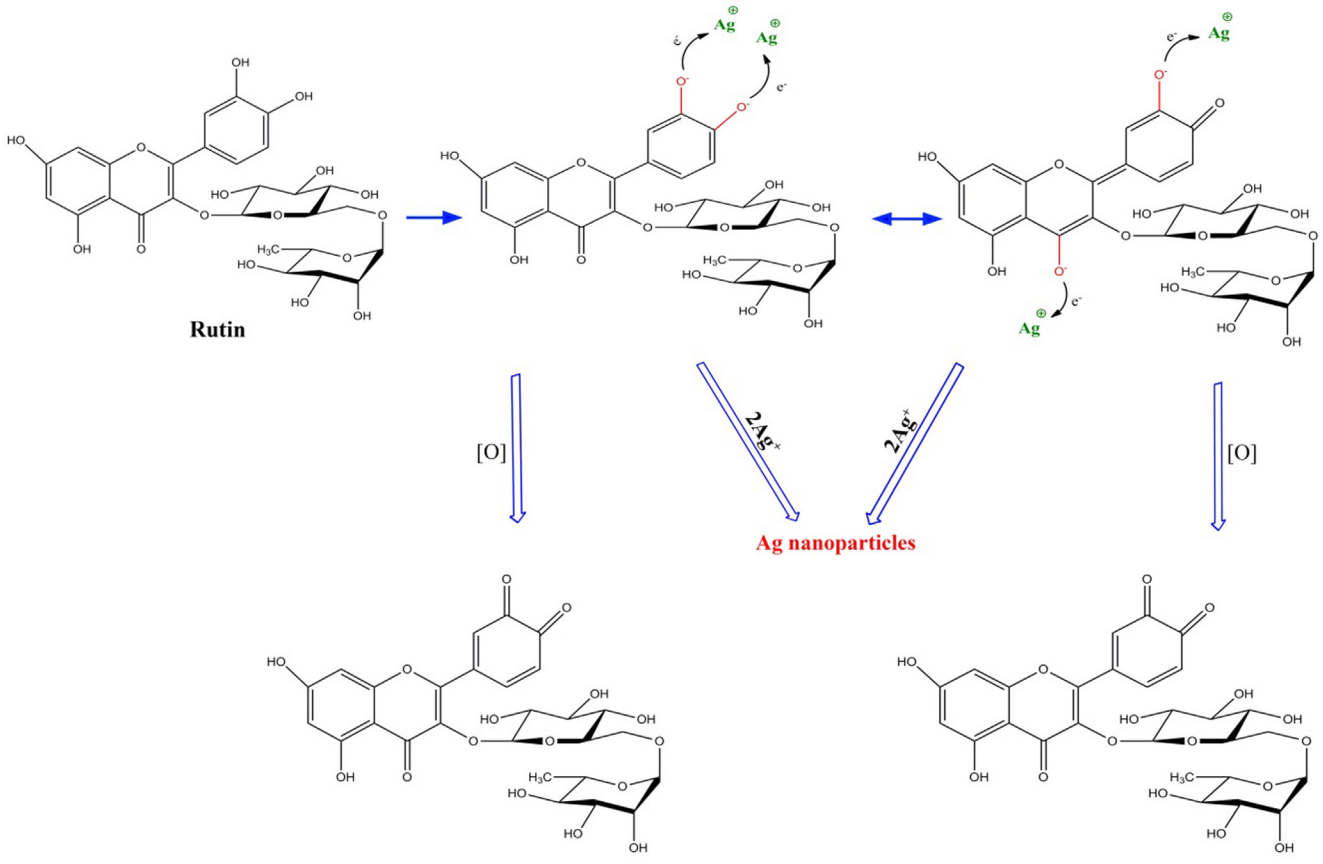

Scheme 1 The possible mechanism of synthesis of silver nanoparticle using *M. sativa* extract.

reaction time, reaching its maximum at 60 min. The band intensity dropped when the contact duration increased to 90 min. This reduction might be explained by sample aggregation. The optimal response time was 60 min based on the spectroscopy results. The reaction was investigated at three different temperatures (room temperature, 65 °C, and 85 °C)

to determine the best temperature for the reaction. According to the UV–Vis absorption diagram (Fig. 2c), the adsorption rate rose with reaction temperature. Additionally, as the reaction temperature increased, the absorption peak shifted to shorter wavelengths, suggesting that the produced nanoparticles became smaller in size. As a result, 85 °C was the optimal temperature for this reaction. These results are consistent with those obtained in previous research (Aboelfetoh et al., 2017). High performance liquid chromatography (HPLC) analysis was used to investigate the mechanism of nanoparticle formation. The HPLC results revealed that the main compounds in the *M. sativa* extract were rutin (18.6 mg g^{-1}), p-coumaric acid (13.1 mg g^{-1}), quercetine (9.7 mg g^{-1}), and chlorogenic acid (6.4 mg g^{-1}). So, we can conclude that the biological activity of extract may attribute to rutin (Scheme. 1).

3.2. XRD analysis

The crystal structure and purity of the produced nanoparticles were determined through XRD analysis. The XRD analysis of sample no. 10 is represented in Fig. 2. As it can be seen, the XRD spectrum contains no impurities, and all peaks correspond to the synthesized silver nanoparticle, indicating the nanoparticles' high purity as per the standard silver diffraction (JCPDS 01–087-0717). XRD analysis reveals peaks at 38.26°, 44.73°, 64.13°, and 77.68°, which correspond to (1 1 1), (2 0 0), (2 2 0), and (3 1 1) Bragg plates, respectively. The XRD analysis of the material confirms earlier findings. The obtained values of crystallite size estimated using Debye-Scherrer equation (Ebrahimzadeh et al., 2019) ($D = n\lambda/\beta\cos\theta$) where D is the average size, λ is the wavelength of the X-ray beam, β is the line broadening at half the maximum intensity and θ is the Bragg angle. According to this equation, the size of AgNPs is approximately 26 nm.

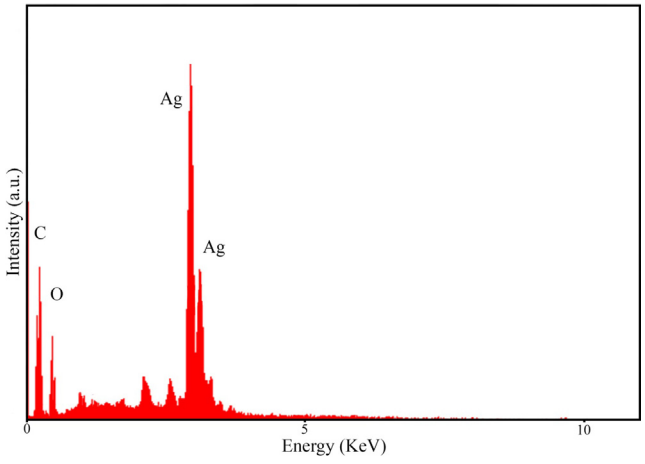

Fig. 3 Energy dispersive X-ray spectroscopy representing the compositional analysis of *MSE*-AgNPs.

3.3. EDS, FESEM and TEM analysis

The energy scattering spectrum (EDS) of *MSE*-AgNPs is portrayed in Fig. 3 (sample no. 10). Silver is the predominant constituent of nanoparticles, as evidenced by a strong signal at 3 keV due to silver's surface plasmon resonance. This EDS analysis revealed that the synthesized nanoparticles contain elements such as C and O, which are linked with the elements found in the *M. sativa* extract involved in the nanoparticle synthesis. The size, morphology, and uniformity of the synthesized nanoparticles may be determined using FESEM images. Fig. 4 illustrates the FESEM images of the synthesized nanoparticles (sample no. 10) at 1 μm, 500 nm, and 200 nm scales. As can be seen in the images, the majority of nanoparticles have a spherical and elliptical morphology with an average diameter of 20–50 nm. Moreover, in some areas, the nanoparticles are stuck together and form an irregular structure, which is attributable to the adhesion of the extracts on the surface of the nanoparticles. TEM analysis was used to evaluate the size and morphology of nanoparticles accurately. The TEM images (Fig. 5) of the synthesized nanoparticles reveal that the synthesized nanoparticles have a spherical morphology in a size range of 15–35 nm. The TEM image explicates the presence of secondary materials, exhibited by the dark shadows on the surface of AgNPs, which may be related to the *M. sativa* extract. Small size, spherical morphology, and uniform structures are characteristic of AgNPs synthesized using *M. sativa* extract, compared to nanoparticles produced in previous research (Rautela et al., 2019).

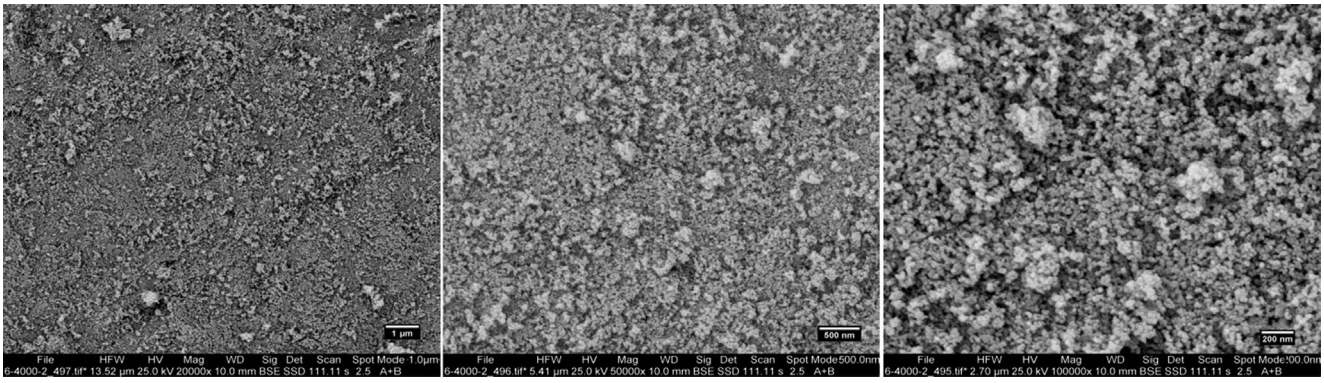

Fig. 4 Field emission scanning electron microscopy (FESEM) images of the biosynthesized AgNPs using *M. sativa* extract at optimum condition (sample no. 10).

3.4. DLS and zeta potential analysis

DLS and zeta potential analyses indicate the particle size (hydrodynamic diameters) and the surface charge of the synthesized nanoparticles, respectively. Fig. 6a displays the DLS histogram of sample no. 10, according to which the hydrodynamic diameter of AgNPs is about 65–130 nm. The particle size analyzed by FESEM was smaller than the particle size obtained in the DLS analysis. This discrepancy in size may be due to the measurement of hydrodynamic diameter in DLS analysis. The surface charge on nanoparticles is critical for avoiding nanoparticle aggregation and boosting their stability (Kim et al., 2013). According to Fig. 6b, the zeta potential of the synthesized nanoparticles was –22.41 mV, which indicates the negative surface charge in the nanoparticles synthesized by the extract.

3.5. FT-IR spectrum

Fig. 7 illustrates the results of FT-IR analysis on *M. sativa* extract and synthesized nanoparticles (sample no. 10). FT-IR analysis revealed the functional groups in *M. sativa* extract and the synthesized nanoparticles. The FT-IR spectra of *M. sativa* extract (Fig. 7a) disclosed that the absorption bands at 3426, 2947, 1665, and 1334 correspond to the O–H stretching vibration, the C–H of hydrocarbon, the C = O of carbonyl bond, and the stretching C = C aromatic ring, respectively (Li et al., 2021). Additionally, Fig. 7b illustrated the FT-IR spectrum of AgNPs produced from *M. sativa* extract. The nanoparticles' adsorption peaks were similar to those of the M. sativa extract. However, they had lower displacement and intensity than those of the *M. sativa* extract, which indicates the effect of *M. sativa* extract functional groups on the formation of nanoparticles (Shaik et al., 2018).

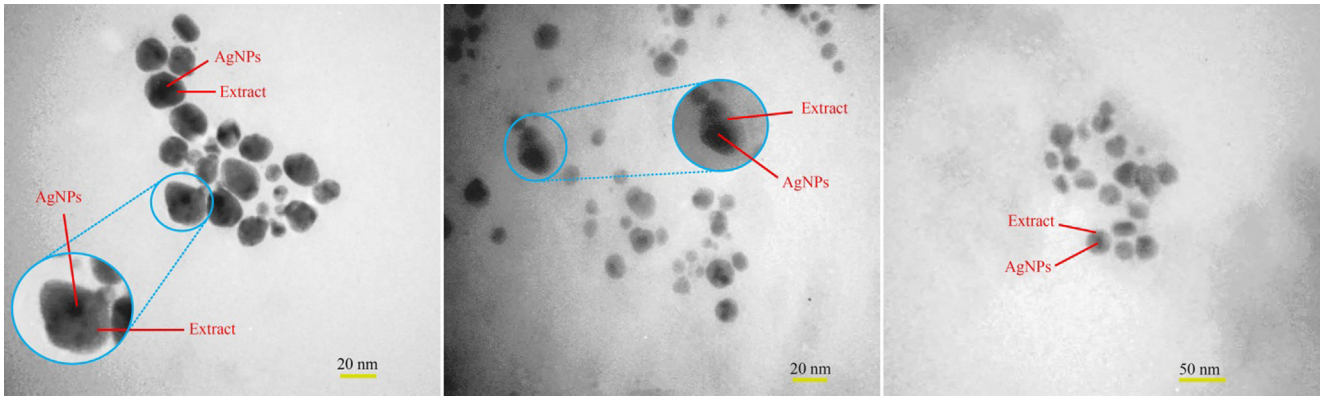

Fig. 5 TEM images of synthesized Ag nanoparticles using *M. sativa* extract (sample no. 10).

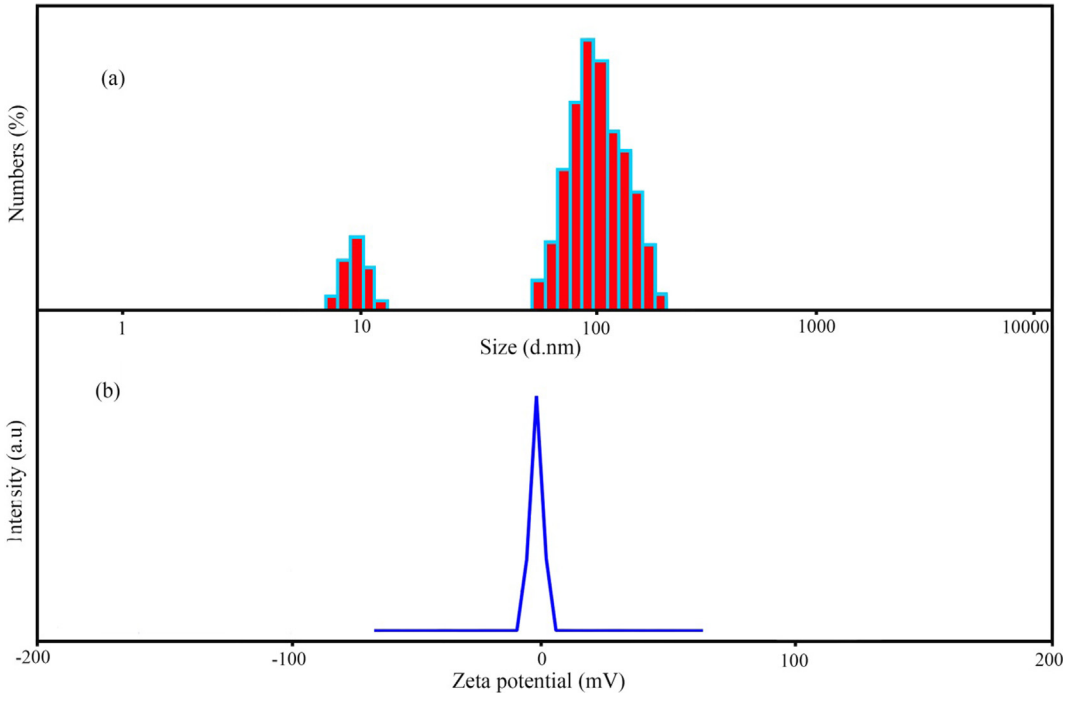

Fig. 6 (a) Dynamic light scattering (DLS) and (b) zeta-potential measurement of *MSE*-AgNPs (sample no. 10).

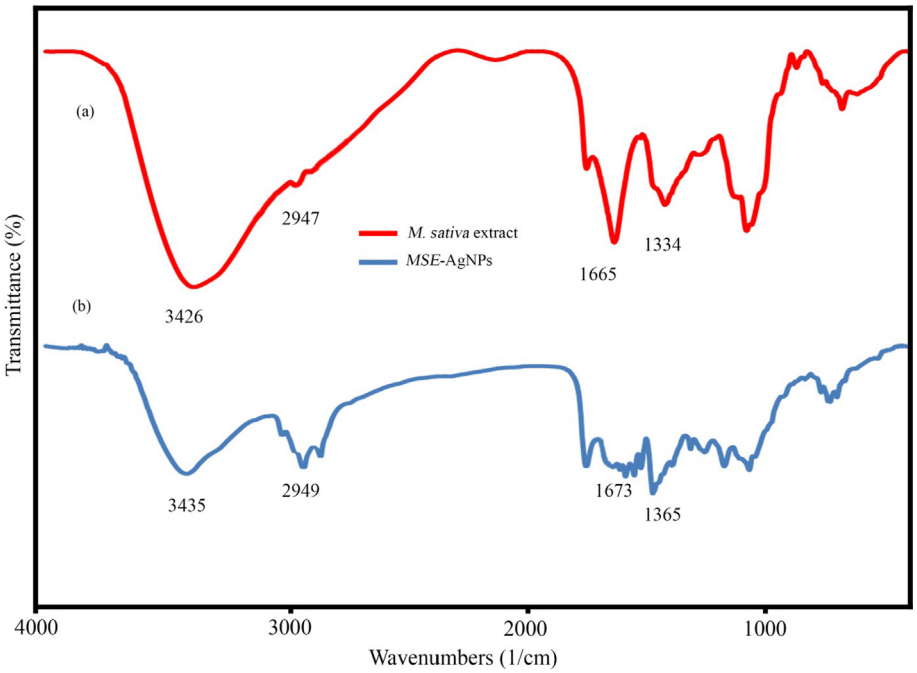

Fig. 7 FT-IR spectrum of *M. sativa* extract (a) and biosynthesized *MSE*-AgNPs (b).

Table 2 MIC and MBC values (μg/ml) of biosynthesis of silver nanoparticles using *M. sativa* extract.

Pathogen	*MSE*-AgNPs		Extract		Ceftriaxone	
	MIC (μg/ml)	MBC (μg/ml)	MIC (mg/ml)	MBC (mg/ml)	MIC (μg/ml)	MBC (μg/ml)
P. aeruginosa ATCC27853	62.5	250	> 50	> 50	97.65	195.31
K. pneumoniae ATCC9997	125	1000	> 50	> 50	12.20	24.41
E. coli ATCC25922	125	250	> 50	> 50	3	6.1
S. epidermidis ATCC12228	1000	2000	> 50	> 50	97.6	390.62
S. faecalis ATCC29212	125	1000	> 50	> 50	195.31	781.25
S. aureus ATCC29213	1000	2000	> 50	> 50	390.62	1562.5

3.6. Antibacterial and antifungal activities

The antibacterial and antifungal activities of *M. sativa* extract and *MSE*-AgNPs are summarized in Table. 2 and Table 3, respectively. According to antibacterial results, *MSE*-AgNPs had excellent antibacterial activity and their antibacterial property was stronger against Gram-negative than against Gram-positive bacteria. Indeed, *P. aeruginosa* exhibited the highest antibacterial activity with MIC and MBC values of 62.5 and 250 μg/mL, respectively. The lowest antibacterial property was noticed in *S. aureus* and *S. epidermidis* with MIC values of 1000 and 1000 μg/mL, respectively. Because gram-negative bacteria have a thinner layer enclosing their membrane and a lipopolysaccharide layer surrounding them, nanoparticles can enter and kill them more readily (Slavin et al., 2017). Additionally, the data indicated that nanoparticles are more efficient against *C. albicans* than bacteria, presumably because fungi belong to the eukaryotic group, while bacteria belong to the prokaryotic group (Marulasiddeshwara et al., 2017). This research found that the methanolic extract of *M. sativa* had no antibacterial effect on the tested bacteria and fungi (up to the 50 mg/mL concentration). This study demonstrates that silver can considerably enhance the antibacterial and antifungal effects of *M. sativa* extract when mixed with it. However, the mechanism through which AgNPs exert antibacterial action is unknown. Our argument is as follows: By and large, the antibacterial activity of nanoparticles is proportional to their shape and size. The smaller the nanoparticles and the larger the surface-to-volume ratio, the more likely the nanoparticles will attach to the microorganism and affect it (Soleimani et al., 2018). Due to their tiny size, nanoparticles may easily infiltrate microorganisms and impair their functioning by connecting to functional regions of key proteins and binding to nucleic acids. Further,

Table 3 MIC and MFC of biosynthesis of silver nanoparticles using *M. sativa* extract.

Fungal strain	*MSE*-AgNPs		Extract		Amphotericin B	
	MIC (μg/ml)	MFC (μg/ml)	MIC (mg/ml)	MFC (mg/ml)	MIC (μg/ml)	MFC (μg/ml)
C. albicans ATCC10231	31.25	31.25	> 50	> 50	4	8

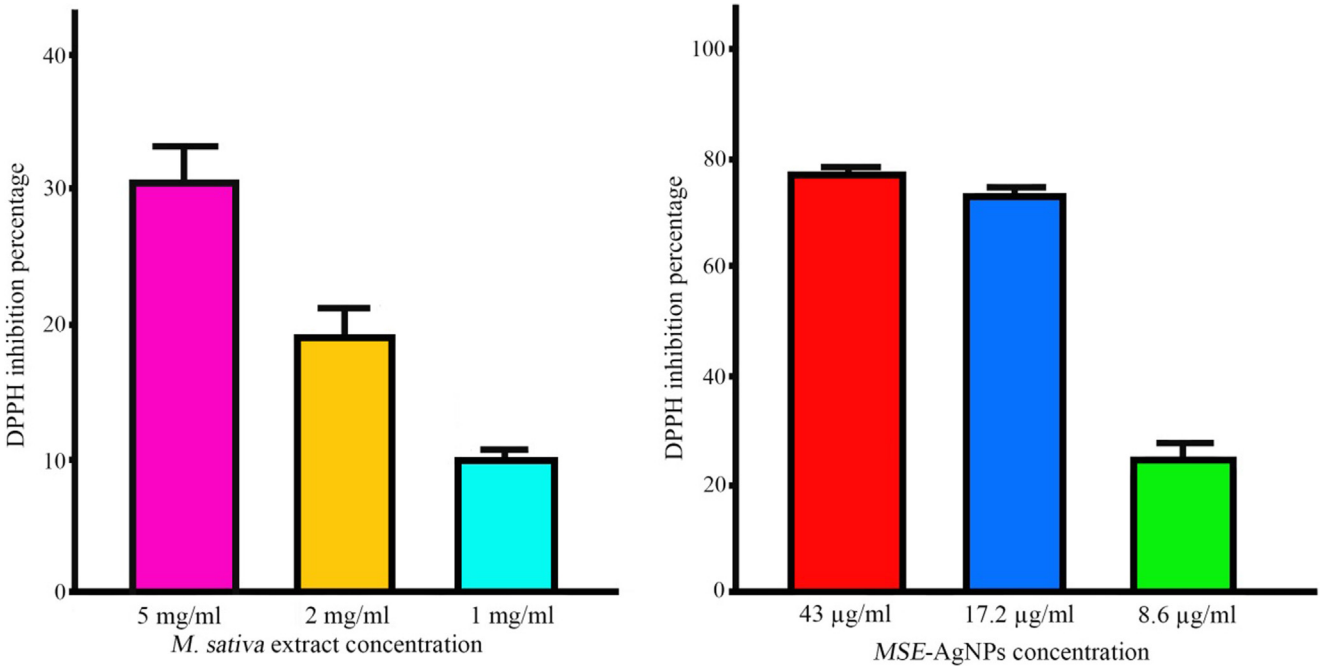

Fig. 8 DPPH inhibition percentage at different concentrations of extract and *MSE*-AgNPs.

they can induce oxidative stress in microorganisms and disrupt the operation of critical microorganism proteins. As microorganisms become more disordered, the function and permeability of the membrane change and microorganisms begin to ruin (Dangi et al., 2020).

3.7. Antioxidant activity

In the organism, oxidative stress arises when the number of free radicals produced exceeds the capacity of antioxidants to neutralize them (Sies, 2020). Oxidative stress is detrimental to many vital molecules in the body, such as nucleic acids, proteins, and lipids. AgNPs and plant extracts have been demonstrated to have a significant level of antioxidant activity in previous investigations (Fouda et al., 2020). There are several ways for assessing a substance's antioxidant activity, one of which is the DPPH method. DPPH is reduced by absorbing hydrogen atoms from the hydroxyl group, resulting in a change in the color of the solution. This color change from purple to yellow indicates the substance's antioxidant capacity (Brand-Williams et al., 1995). The present study investigated the percentage of DPPH inhibition as seen by nanoparticles and alfalfa extract in three concentrations (Fig. 8). The results demonstrated a direct link between nanoparticle concentration and DPPH inhibition percentage, with higher concentrations resulting in higher DPPH inhibition percentages. The percentage of DPPH inhibition rose from 25% to 78% when the nanoparticle concentration was raised from 8.6 to 43 μg/mL. By increasing the concentration of *M. sativa* extract from 1

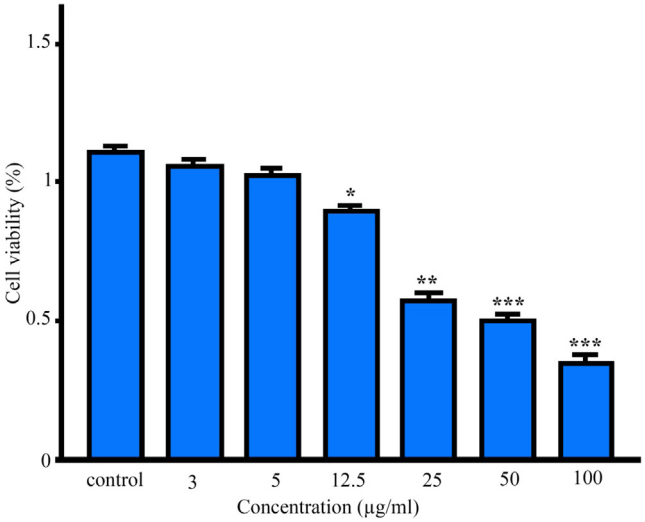

Fig. 9 The results of the MTT assay in human fibroblasts cells treated with *MSE*-AgNPs after 24 h. Results were reported as survival percentage compared to control samples ($p < 0.001$***, $p < 0.01$**, $p < 0.05$*).

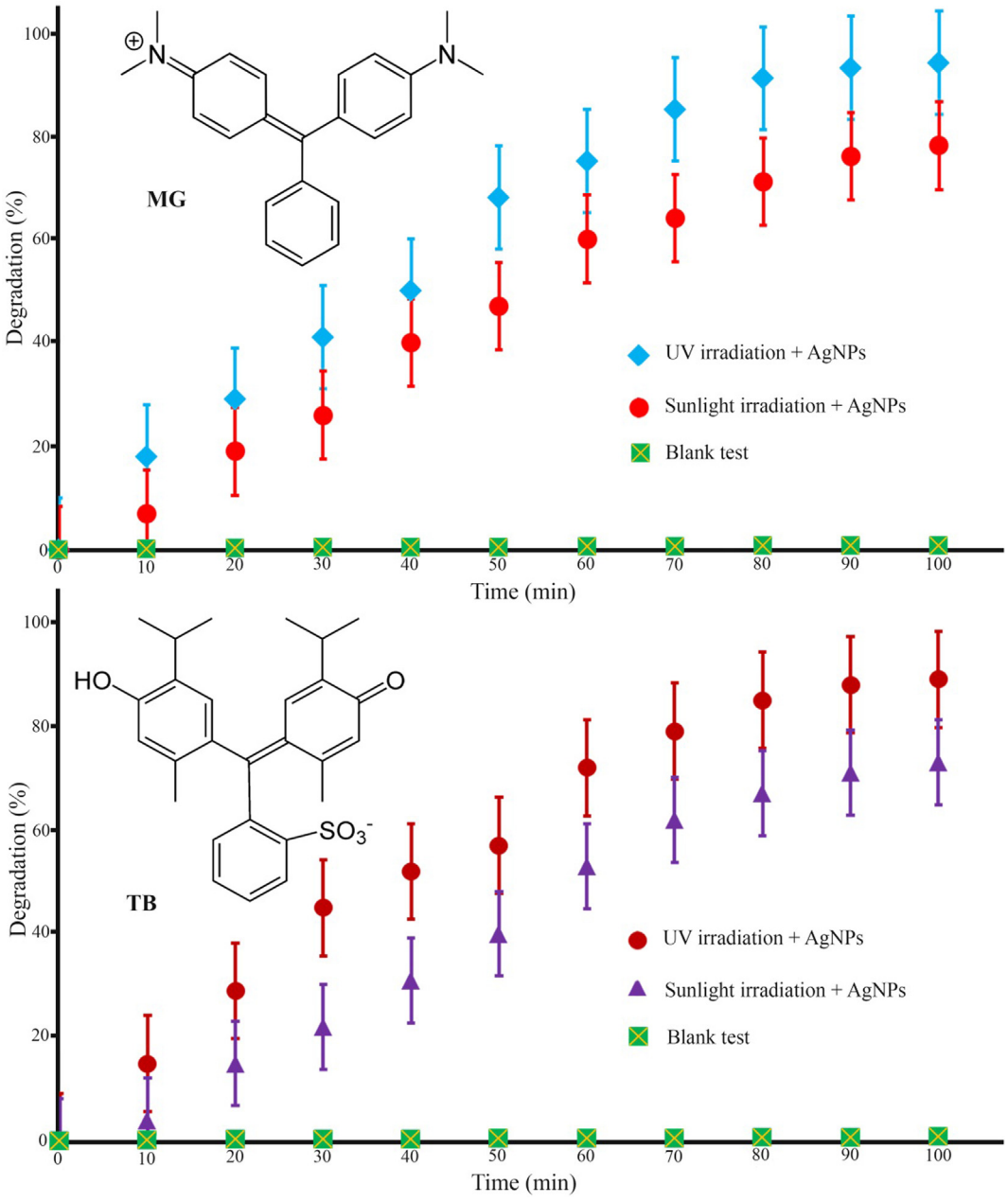

Fig. 10 Photocatalytic degradation of thymol blue (TB) and malachite green (MG) organic pollutants by *MSE*-AgNPs.

to 5 mg/mL, the percentage of DPPH inhibition rose from 9 to 32%. Our results reveal that using *M. sativa* extract to synthesize AgNPs significantly improves their antioxidant properties. Consistent with our findings, Jalilian *et al.* discovered that AgNPs generated from *Allium ampeloprasum* extract had greater antioxidant activity than AgNPs synthesized from pure *Allium ampeloprasum* extract (Jalilian et al., 2020).

3.8. Cytotoxicity of biogenic silver nanoparticles

This study analyzed the toxicity of AgNPs synthesized using M. sativa extract against human fibroblasts at 3, 5, 12.5, 25, 50, 100 µg/mL concentrations via the MTT colorimetric method. Moreover, cell viability percentage was assessed after 24 h. The presence of cells was assessed after 24 h. Treatment of human fibroblasts with different concentrations of AgNPs showed that the cytotoxicity of the synthesized AgNPs was dose-dependent. Indeed, the most cytotoxic effects were observed at concentrations of 50 µg/mL and 100 µg/ml, and the amount of inhibitory concentration (IC50) was 18.22 µg/mL (Fig. 9).

3.9. Photocatalytic activity

The photocatalytic activity of biogenic AgNPs was investigated by observing the degradation of cationic and anionic organic pollutants, such as thymol blue (TB) and malachite green (MG), in an aqueous solution under UV and sunlight

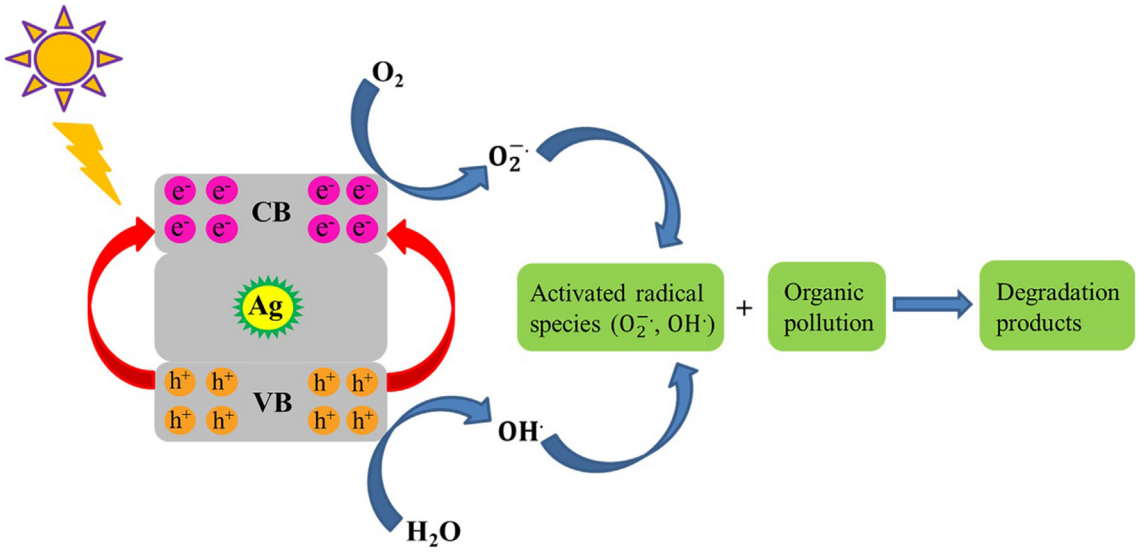

Scheme 2 Mechanism of photocatalytic degradation of organic pollutions by *MSE*-AgNPs.

radiations. Fig. 10 illustrates the photocatalytic degradation of TB and MG contaminants. In the absence of *MSE*-AgNPs or light, virtually no pollutants were degraded after 100 min, indicating that the self-degradation component was irrelevant. Fig. 10 depicts the details of the degradation performance of TB and MG pollutants under UV and sunlight irradiations. As can be seen, the contaminant degradation percentages of the MG dye are nearly 94.37% and 82.65% under UV and sunlight irradiation after 100 min, respectively. Additionally, a review of the catalytic data revealed that TB was degraded by 90.12 percent and 74.22 percent in 100 min when exposed to UV and sunlight, respectively. Comparison of the results indicated that in the presence of AgNPs, a pollutant with a positive charge (cationic) degraded more rapidly than a dye with a negative charge (anionic). The mechanism of pollutions via optimized biogenic AgNPs by superoxide anion and hydroxyl radicals is presented below (Scheme. 2):

$$Ag + h\nu \rightarrow Ag + e^{-}_{CB} + h^{+}_{VB} \quad (6)$$

$$h^{+}_{VB} + H2O \rightarrow OH^{\cdot} + H+ \quad (7)$$

$$e^{-}_{CB} + O_2 \rightarrow O^{-}_{2} \quad (8)$$

$$O^{-}_{2} + H+ \rightarrow HO^{\cdot}_{2} \quad (9)$$

$$\text{Contaminant} + OH^{\cdot} \rightarrow \text{degradationsample} \quad (10)$$

$$\text{Contaminant} + h^{+}_{VB} \rightarrow \text{oxidationsample} \quad (11)$$

$$\text{Contaminant} + e^{-}_{CB} \rightarrow \text{reductionsample} \quad (12)$$

4. Conclusion

In conclusion, metallic AgNPs were effectively synthesized from *M. sativa* extract in a cost-effective and straightforward biosynthetic approach. The produced nanoparticles were characterized using various analyses. The TEM analysis confirmed that the prepared *MSE*-AgNPs was highly pure and had a regular spherical morphology with an average size of 15–35 nm. Additionally, the photocatalytic degradation, antifungal, antibacterial, and cytotoxic activities were determined. The photocatalytic results showed that *MSE*-AgNPs could efficiently degrade thymol blue (90.12%) and malachite green (94.37%) dyes under UV irradiation. Furthermore, *MSE*-AgNPs exhibited effective antifungal and antibacterial activities against Gram-positive and Gram-negative bacteria. Examination of the toxicity of AgNPs revealed that the most cytotoxic effects (IC50 18.22 µg/mL) were observed at 50 and 100 µg/mL concentrations. The synthesized silver nanoparticles potential catalytic and biological activities make it a highly efficient candidate for environmental and biomedical applications.

Declaration of Competing Interest

The authors declare that they have no known competing financial interests or personal relationships that could have appeared to influence the work reported in this paper.

Acknowledgment

In this investigation, the entire procedures were conducted according to the Helsinki Declaration and ethical standards of the institutional research committee. The ethics code was taken from Birjand University of Medical Sciences (IR.BUMS.REC.1400.046).

References

Ghoreishi, S.M., Khalaj, A., Bitarafan-Rajabi, A., Azar, A.D., Ardestani, M.S., Assadi, A., 2017. Novel 99mTc-Radiolabeled Anionic Linear Globular PEG-Based Dendrimer-Chlorambucil: Non-Invasive Method for In-Vivo Biodistribution. Drug Res (Stuttg) 67 (3), 149–155.

Shirzadi-Ahodashti, M., Ebrahimzadeh, M.A., Ghoreishi, S.M., Naghizadeh, A., Mortazavi-Derazkola, S., 2020. Facile and eco-benign synthesis of a novel $MnFe_2O_4$@SiO_2@Au magnetic nanocomposite with antibacterial properties and enhanced photocatalytic activity under UV and visible-light irradiations. Appl. Organomet. Chem. 34, (5) e5614.

Zamarchi, F., Vieira, I.C., 2021. Determination of paracetamol using a sensor based on green synthesis of silver nanoparticles in plant extract. J. Pharm. Biomed. Anal. 196, 113912.
Ahmadi, S., Rahdar, A., Igwegbe, C.A., Mortazavi-Derazkola, S., Banach, A.M., Rahdar, S., Singh, A.K., Rodriguez-Couto, S., Kyzas, G.Z., 2020. Praseodymium-doped cadmium tungstate ($CdWO_4$) nanoparticles for dye degradation with sonocatalytic process. Polyhedron 190, 114792.
Mohammadzadeh, P., Shafiee Ardestani, M., Mortazavi-Derazkola, S., Bitarafan-Rajabi, A., Ghoreishi, S.M., 2019. PEG-Citrate dendrimer second generation: is this a good carrier for imaging agents In Vitro and In Vivo ? IET Nanobiotechnol. 13 (6), 560–564.
Liu, X., Bing, T., Shangguan, D., 2017. Microbead-Based Platform for Multiplex Detection of DNA and Protein. ACS Appl. Mater. Interfaces 9 (11), 9462–9469.
Abbott Chalew, T.E., Ajmani, G.S., Huang, H., Schwab, K.J., 2013. Evaluating nanoparticle breakthrough during drinking water treatment. Environ. Health Perspect. 121 (10), 1161–1166.
Watermann, A., Brieger, J., 2017. Mesoporous Silica Nanoparticles as Drug Delivery Vehicles in Cancer. Nanomaterials 7 (7), 189.
Chen, H., Zhou, K., Zhao, G., 2018. Gold nanoparticles: From synthesis, properties to their potential application as colorimetric sensors in food safety screening. Trends Food Sci. Technol. 78, 83–94.
Kim, J.S., Kuk, E., Yu, K.N., Kim, J.-H., Park, S.J., Lee, H.J., Kim, S.H., Park, Y.K., Park, Y.H., Hwang, C.-Y., Kim, Y.-K., Lee, Y.-S., Jeong, D.H., Cho, M.-H., 2007. Antimicrobial effects of silver nanoparticles, Nanomedicine: Nanotechnology. Biology and Medicine 3 (1), 95–101.
Ravichandran, V., Vasanthi, S., Shalini, S., Shah, S.A.A., Tripathy, M., Paliwal, N., 2019. Green synthesis, characterization, antibacterial, antioxidant and photocatalytic activity of Parkia speciosa leaves extract mediated silver nanoparticles. Results Phys. 15, 102565.
Bagherzade, G., Tavakoli, M.M., Namaei, M.H., 2017. Green synthesis of silver nanoparticles using aqueous extract of saffron (Crocus sativus L.) wastages and its antibacterial activity against six bacteria. Asian Pacific Journal of Tropical Biomedicine 7 (3), 227–233.
Ebrahimzadeh, M.A., Naghizadeh, A., Mohammadi-Aghdam, S., Khojasteh, H., Ghoreishi, S.M., Mortazavi-Derazkola, S., 2020. Enhanced catalytic and antibacterial efficiency of biosynthesized Convolvulus fruticosus extract capped gold nanoparticles (CFE@AuNPs). J. Photochem. Photobiol., B 209, 111949.
Khoshnamvand, M., Ashtiani, S., Liu, J., 2020. Acute toxicity of gold nanoparticles synthesized from macroalga Saccharina japonica towards Daphnia magna. Environ. Sci. Pollut. Res. 27 (17), 22120–22126.
Shirzadi-Ahodashti, M., Mizwari, Z.M., Hashemi, Z., Rajabalipour, S., Ghoreishi, S.M., Mortazavi-Derazkola, S., Ebrahimzadeh, M. A., 2021. Discovery of high antibacterial and catalytic activities of biosynthesized silver nanoparticles using C. fruticosus (CF-AgNPs) against multi-drug resistant clinical strains and hazardous pollutants. Environ. Technol. Innovation 23, 101607.
Huo, C., Khoshnamvand, M., Liu, C., Wang, H., Liu, P., Yuan, C.-G., 2019. Roles of silver nanoparticles adsorbed ions and nanoparticles' size in antimicrobial activity of biosynthesized silver nanoparticles. Mater. Res. Express 6 (12), 1250a6.
Zhou, X., Wang, B., Jia, Z., Zhang, X., Liu, X., Wang, K., Xu, B., Wu, G., 2021. Dielectric behavior of Fe_3N@C composites with green synthesis and their remarkable electromagnetic wave absorption performance. J. Colloid Interface Sci. 582, 515–525.
V. K, V. A, M. P, S. S, M. S, S. S, Green inspired synthesis of ZnO nanoparticles and its characterizations with biofilm, antioxidant, anti-inflammatory, and anti-diabetic activities, Journal of Molecular Structure 1255 (2022) 132420.
Awwad, A.M., Amer, M.W., Salem, N.M., Abdeen, A.O., 2020. Green synthesis of zinc oxide nanoparticles (ZnO-NPs) using Ailanthus altissima fruit extracts and antibacterial activity.
Mittal, J., Batra, A., Singh, A., Sharma, M.M., 2014. Phytofabrication of nanoparticles through plant as nanofactories. Adv. Nat. Sci.: Nanosci. Nanotechnol. 5, (4) 043002.
AlSalhi, M.S., Elangovan, K., Ranjitsingh, A.J.A., Murali, P., Devanesan, S., 2019. Synthesis of silver nanoparticles using plant derived 4-N-methyl benzoic acid and evaluation of antimicrobial, antioxidant and antitumor activity. Saudi J. Biological Sciences 26 (5), 970–978.
Ahmed, S., Ahmad, M., Swami, B.L., Ikram, S., 2016. A review on plants extract mediated synthesis of silver nanoparticles for antimicrobial applications: A green expertise. J. Adv. Res. 7 (1), 17–28.
Shirzadi-Ahodashti, M., Mortazavi-Derazkola, S., Ebrahimzadeh, M. A., 2020. Biosynthesis of noble metal nanoparticles using crataegus monogyna leaf extract (CML@X-NPs, X= Ag, Au): Antibacterial and cytotoxic activities against breast and gastric cancer cell lines. Surf. Interfaces 21, 100697.
Ebrahimzadeh, M.A., Hashemi, Z., Mohammadyan, M., Fakhar, M., Mortazavi-Derazkola, S., 2021. In vitro cytotoxicity against human cancer cell lines (MCF-7 and AGS), antileishmanial and antibacterial activities of green synthesized silver nanoparticles using Scrophularia striata extract. Surf. Interfaces 23, 100963.
Hidayat, M.I., Adlim, M., Maulana, I., Suhartono, S., Hayati, Z., Bakar, N.H.H.A., 2022. Green synthesis of chitosan-stabilized silver-colloidal nanoparticles immobilized on white-silica-gel beads and the antibacterial activities in a simulated-air-filter. Arabian J. Chem. 15, (2) 103596.
Hamelian, M., Zangeneh, M.M., Amisama, A., Varmira, K., Veisi, H., 2018. Green synthesis of silver nanoparticles using Thymus kotschyanus extract and evaluation of their antioxidant, antibacterial and cytotoxic effects. Appl. Organomet. Chem. 32, (9) e4458.
Alfuraydi, A.A., Devanesan, S., Al-Ansari, M., AlSalhi, M.S., Ranjitsingh, A.J., 2019. Eco-friendly green synthesis of silver nanoparticles from the sesame oil cake and its potential anticancer and antimicrobial activities. J. Photochem. Photobiol., B 192, 83–89.
Mehwish, H.M., Rajoka, M.S.R., Xiong, Y., Cai, H., Aadil, R.M., Mahmood, Q., He, Z., Zhu, Q., 2021. Green synthesis of a silver nanoparticle using Moringa oleifera seed and its applications for antimicrobial and sun-light mediated photocatalytic water detoxification. J. Environ. Chem. Eng. 9, (4) 105290.
Basafa, M., Taherian, M., 2009. A study of agronomic and morphological variations in certain alfalfa (Medicago sativa L.) ecotypes of the cold region of Iran. Asian J. Plant Sciences.
Shi, S., Nan, L., Smith, K.F., 2017. The Current Status, Problems, and Prospects of Alfalfa (Medicago sativa L.). Breeding in China, Agronomy 7 (1), 1.
Hashemi, Z., Mohammadyan, M., Naderi, S., Fakhar, M., Biparva, P., Akhtari, J., Ebrahimzadeh, M.A., 2021. Green synthesis of silver nanoparticles using Ferula persica extract (Fp-NPs): Characterization, antibacterial, antileishmanial, and in vitro anticancer activities. Mater. Today Commun. 27, 102264.
Brand-Williams, W., Cuvelier, M.E., Berset, C., 1995. Use of a free radical method to evaluate antioxidant activity. LWT - Food Science Technology 28 (1), 25–30.
Naghizadeh, A., Mizwari, Z.M., Ghoreishi, S.M., Lashgari, S., Mortazavi-Derazkola, S., Rezaie, B., 2021. Biogenic and eco-benign synthesis of silver nanoparticles using jujube core extract and its performance in catalytic and pharmaceutical applications: Removal of industrial contaminants and in-vitro antibacterial and anticancer activities. Environ. Technol. Innovation 23, 101560.
Anand, K., Kaviyarasu, K., Muniyasamy, S., Roopan, S.M., Gengan, R.M., Chuturgoon, A.A., 2017. Bio-Synthesis of Silver Nanoparticles Using Agroforestry Residue and Their Catalytic Degradation

for Sustainable Waste Management. J. Cluster Sci. 28 (4), 2279–2291.
Aboelfetoh, E.F., El-Shenody, R.A., Ghobara, M.M., 2017. Eco-friendly synthesis of silver nanoparticles using green algae (Caulerpa serrulata): reaction optimization, catalytic and antibacterial activities. Environ. Monit. Assess. 189 (7), 349.
Ebrahimzadeh, M.A., Mortazavi-Derazkola, S., Zazouli, M.A., 2019. Eco-friendly green synthesis and characterization of novel Fe_3O_4/SiO_2/Cu_2O–Ag nanocomposites using Crataegus pentagyna fruit extract for photocatalytic degradation of organic contaminants. J. Mater. Sci.: Mater. Electron. 30 (12), 10994–11004.
Rautela, A., Rani, J., Debnath, M., 2019. Green synthesis of silver nanoparticles from Tectona grandis seeds extract: characterization and mechanism of antimicrobial action on different microorganisms. J. Anal. Sci. Technol. 10 (1), 5.
Kim, S.T., Saha, K., Kim, C., Rotello, V.M., 2013. The Role of Surface Functionality in Determining Nanoparticle Cytotoxicity. Acc. Chem. Res. 46 (3), 681–691.
Li, S., Al-Misned, F.A., El-Serehy, H.A., Yang, L., 2021. Green synthesis of gold nanoparticles using aqueous extract of Mentha Longifolia leaf and investigation of its anti-human breast carcinoma properties in the in vitro condition. Arabian J. Chem. 14, (2) 102931.
Shaik, M.R., Khan, M., Kuniyil, M., Al-Warthan, A., Alkhathlan, H. Z., Siddiqui, M.R.H., Shaik, J.P., Ahamed, A., Mahmood, A., Khan, M., Adil, S.F., 2018. Plant-Extract-Assisted Green Synthesis of Silver Nanoparticles Using Origanum vulgare L. Extract and Their Microbicidal Activities. Sustainability 10 (4), 913.
Slavin, Y.N., Asnis, J., Häfeli, U.O., Bach, H., 2017. Metal nanoparticles: understanding the mechanisms behind antibacterial activity. J Nanobiotechnology 15 (1), 65.
Marulasiddeshwara, M.B., Dakshayani, S.S., Sharath Kumar, M.N., Chethana, R., Raghavendra Kumar, P., Devaraja, S., 2017. Facile-one pot-green synthesis, antibacterial, antifungal, antioxidant and antiplatelet activities of lignin capped silver nanoparticles: A promising therapeutic agent. Mater. Sci. Eng., C 81, 182–190.
Soleimani, F.F., Saleh, T., Shojaosadati, S.A., Poursalehi, R., 2018. Green Synthesis of Different Shapes of Silver Nanostructures and Evaluation of Their Antibacterial and Cytotoxic Activity. BioNanoScience 8 (1), 72–80.
Dangi, S., Gupta, A., Gupta, D.K., Singh, S., Parajuli, N., 2020. Green synthesis of silver nanoparticles using aqueous root extract of Berberis asiatica and evaluation of their antibacterial activity. Chem. Data Collect. 28, 100411.
Sies, H., 2020. Oxidative Stress: Concept and Some Practical Aspects. Antioxidants 9 (9), 852.
Fouda, A., Hassan, S.-E.-D., Abdo, A.M., El-Gamal, M.S., 2020. Antimicrobial, Antioxidant and Larvicidal Activities of Spherical Silver Nanoparticles Synthesized by Endophytic Streptomyces spp. Biol. Trace Elem. Res. 195 (2), 707–724.
Jalilian, F., Chahardoli, A., Sadrjavadi, K., Fattahi, A., Shokoohinia, Y., 2020. Green synthesized silver nanoparticle from Allium ampeloprasum aqueous extract: Characterization, antioxidant activities, antibacterial and cytotoxicity effects. Adv. Powder Technol. 31 (3), 1323–1332.